HHS Public Access

Author manuscript

Biomater Sci. Author manuscript; available in PMC 2021 January 15.

Published in final edited form as:

Biomater Sci. 2020 July 21; 8(14): 3935–3943. doi:10.1039/d0bm00683a.

Affinity of plant viral nanoparticle potato virus X (PVX) towards malignant B cells enables cancer drug delivery†

Sourabh Shukla[‡,a], **Anne Jessica Roe**[‡,b], **Ruifu Liu**[b], **Frank A. Veliz**[c], **Ulrich Commandeur**[d], **David N. Wald**[b], **Nicole F. Steinmetz**[a,e,f,g,h]

[a]Department of NanoEngineering, University of California San Diego, La Jolla, California, 92093, USA.

[b]Department of Pathology, Case Western Reserve University, Cleveland, Ohio 44106, USA.

[c]Department of Biomedical Engineering, Case Western Reserve University, Cleveland, Ohio 44106, USA

[d]Department of Molecular Biotechnology, RWTH-Aachen University, Aachen 52064, Germany

[e]Department of Bioengineering, University of California San Diego, La Jolla, California, 92093, USA

[f]Department of Radiology, University of California San Diego, La Jolla, California, 92093, USA

[g]Moores Cancer Center, University of California San Diego, La Jolla, California, 92093, USA

[h]Center for Nano-ImmunoEngineering, University of California San Diego, La Jolla, California, 92093, USA

Abstract

Non-Hodgkin's B cell lymphomas (NHL) include a diverse set of neoplasms that constitute ~90% of all lymphomas and the largest subset of blood cancers. While chemotherapy is the first line of treatment, the efficacy of contemporary chemotherapies is hampered by dose-limiting toxicities. Partly due to suboptimal dosing, ~40% of patients exhibit relapsed or refractory disease. Therefore more efficacious drug delivery systems are urgently needed to improve survival of NHL patients. In this study we demonstrate a new drug delivery platform for NHL based on the plant virus Potato virus X (PVX). We observed a binding affinity of PVX towards malignant B cells. In a metastatic mouse model of NHL, we show that systemically administered PVX home to tissues harboring malignant B cells. When loaded with the chemotherapy monomethyl auristatin (MMAE), the PVX nanocarrier enables effective delivery of MMAE to human B lymphoma cells in a NHL mouse model leading to inhibition of lymphoma growth *in vivo* and improved survival. Thus, PVX nanoparticle is a promising drug delivery platform for B cell malignancies.

†Electronic supplementary information (ESI) available. See DOI: 10.1039/d0bm00683a

nsteinmetz@ucsd.edu.

‡These authors contributed equally.

Conflicts of interest

There are no conflicts to declare.

Introduction

Non-Hodgkin's Lymphoma (NHL) is the most frequent hematologic malignancy with an estimated 72 240 new cases diagnosed in the United States in 2017.[1] NHL is a heterogeneous group of cancers that arise from lymphoid cells. The vast majority (~90%) of NHL's are derived from B cells. Though advances have been made in the treatment of B cell lymphomas over the last 30 years, greater than 30% of patients still die within 5 years of diagnosis.[2] Systemic chemotherapy is the first line of treatment for lymphoma. Standard upfront treatment involves R-CHOP chemoimmunotherapy (rituximab, cyclophosphamide, doxorubicin, vincristine and prednisone). However, clinical efficacies are hampered by dose-limiting toxicities.[3] As a consequence, insufficient dosing can lead to partial remission and selection pressure leading to development of drug resistance.[3,4] Unfortunately, ~40% of NHL patients exhibit relapsed or refractory disease after front-line treatment and the relapsed lymphomas are typically cross resistant to many chemotherapeutics.[5,6] Attempts at dose escalation have led to significant systemic toxicities without clinical benefits.[3,4]

Drug delivery approaches hold promise to reduce systemic adverse effects associated with chemotherapy; and drug targeting can achieve larger chemotherapy doses to be delivered to the cancer cells. Antibody–drug conjugates (ADCs) are the current mainstay of lymphoma drug delivery, where mono-clonal antibodies targeting tumor antigens deliver chemotherapy selectively to cancer cells.[7,8] Currently, four ADCs are FDA approved for clinical use and efforts are ongoing towards improving the manufacturing process, drug payloads and broadening the repertoire of candidate drugs.[7,9] ADCs also face physiological complexities including targeted receptor heterogeneity and down regulation in tumors, recycling of ADCs with receptors leading to non-specific drug release and premature release of drugs due to typically long circulation half-lives of these antibodies (days to weeks).[7,10] Therefore, development of alternative and/or improved drug delivery vehicles is a field of great interest.

Nanoparticle-based drug delivery systems can incorporate a broad range of chemotherapy using a range of established bioconjugation strategies and improve drug stability and bioavailability.[11,12] Several drug delivery platforms including silica nanoparticles,[13] targeted lipid nanoparticles,[14] lipid polymeric nanocarriers[15] and platelets[16] have been evaluated for lymphoma drug delivery applications.

In this study, we tested the utility of a filamentous plant virus nanotechnology as a NHL drug delivery platform. Plant viruses are naturally occurring nanomaterials that have been increasingly used for biomedical applications including preclinical imaging, drug-delivery, vaccines and cancer immunotherapy. With highly organized protein capsids, plant viral nanoparticles offer excellent scaffolds for multivalent display of contrast agents, therapeutic payloads and epitopes.[17–22] Additionally, plant viral nanoparticles are biocompatible, biodegradable and non-infectious in mammalian cells. Potato virus X (PVX) is a filamentous plant virus measuring 513 nm × 13 nm that has demonstrated enhanced homing and penetration in solid tumors.[23,24] In previous work, we have observed that PVX homes to solid tumors when administered systemically in tumor bearing mice and traffics to B cell follicles in spleen and lymph nodes in healthy mice.[24,25] Therefore, we set out to assess targeting of NHL. Specifically, we tested homing of PVX to malignant B cells *in vitro* and in

mouse models of orthotropic human lymphoma. Furthermore, we prepared PVX nanoparticles loaded with the cytotoxic drug, monomethyl auristatin (MMAE), and investigated its potential for drug delivery targeting NHL.

Experimental

Cell lines and reagents

Cell lines (Raji, Daudi, OCI-AML3, OVCAR-3, HCT116) were maintained in RPMI media supplemented with 10% (v/v) cosmic serum (GE Healthcare) and 1% (v/v) penicillin–streptomycin (GE Healthcare). Luciferase-expressing Raji cells (Rajiluc) were generated by stably transfecting Raji cells using the plasmid pLenti-CMV V5-luciferase (Addgene) using methods as previously reported.[26] PBMCs were isolated from healthy donor blood obtained from the Hematopoietic Biorepository and Cellular Therapy Core at CWRU and maintained in RPMI media supplemented with 10% (v/v) cosmic serum (GE Healthcare) and 100 U mL^{-1} Penicillin with 100 μg mL^{-1} Streptomycin (GE Healthcare). Monomethyl auristatin E (MMAE) and vcMMAE were obtained from MedChemExpress, (Monmouth Junction, NJ).

PVX production

PVX was propagated in *Nicotiana benthamiana* plants and purified according to our established protocols.[27] The yields from 100 g of infected leaves were ~10 to 20 mg of pure PVX.

Chemical bioconjugation of Cy5 dyes

PVX-Cy5 fluorescent particles were synthesized by coupling NHS-Sulfo-Cy5 or Maleimide-Sulfo-Cy5 (Lumiprobe) to PVX *via* lysine or cysteine residues, respectively. PVX (at 2 mg mL^{-1}) was reacted with 0.5 molar excess of sulfo-Cy5 dye/CP in 0.1 M potassium phosphate buffer (pH 7.0) supplemented with 10% (v/v) DMSO on a rotisserie overnight at room temperature. Dye labeled PVX was purified by ultracentrifugation at 112 000*g* for 3 hours over a 30% (w/v) sucrose cushion. The resulting pellet was resuspended in 0.1 M potassium phosphate buffer pH 7. Post-purification, PVX concentration and number of Cy5/PVX in the resulting PVX-Lys-Cy5 (PVX-Cy5) and PVX-Cys-Cy5 particles were determined by UV-vis spectroscopy using the Beer–Lambert law and the PVX and Sulfo-Cy5-specific extinction coefficients of 2.97 mL mg^{-1} cm^{-1} at 260 nm and 271 000 M^{-1} cm^{-1} at 647 nm, respectively. Particle integrity was verified using size exclusion chromatography using a Superose6 column on the ÄKTA Explorer chromatography system (GE Healthcare).

Chemical bioconjugation of vcMMAE

vcMMAE (MedChem Express) was conjugated to PVX *via* the sulfhydryl side chains on the cysteine residues using the maleimide chemistry. 7500 molar excess of vcMMAE was reacted overnight with PVX at a protein concentration of 1 mg mL^{-1} in presence of 10% (v/v) DMSO. PVX–vcMMAE was purified *via* ultracentrifugation at 112 000*g* for 3 hours over 30% sucrose cushion to remove unbound vcMMAE. The recovered PVX–vcMMAE pellet was resuspended in 0.1 M potassium phosphate buffer pH 7 and dialyzed against 0.1 M phosphate buffer. Purified PVX–vcMMAE were imaged by transmission electron

microscopy TEM (FEI Tecnai Spirit G2 BioTWIN Transmission Electron Microscope) for particle stability and analyzed by dynamic light scattering (DLS) to rule out particle aggregation. Drug loading was quantified by SDS-PAGE (4–12% NuPAGE gels, 1× MOPS running buffer, Invitrogen) followed by densitometry analysis performed using the band analysis tool in ImageJ software (https://imagej.net/Fiji).

PVX biodistribution and intra-tissue localization

All animal experiments were carried out in accordance with the Case Western Reserve University's Institutional Animal Care and Use Committee (IACUC). Male and female NOD/SCID/IL2-Rγ (NSG) mice (7 weeks; $n = 3$) were injected with 5×10^6 Raji-luc cells intravenously. Tumor progression was monitored using *in vivo* bioluminescence imagine on IVIS Spectrum imager (PerkinElmer). On day 27 from tumor challenge, mice were injected intraperitoneally (i.p.) with PVX-Cy5 (5 mg kg^{-1}) in PBS (200 μL) and then imaged using IVIS spectrum after 24 hours for bioluminescence from Raji-luc cells and fluorescence from PVX-Cy5 particles. Post-imaging mice were sacrificed, and harvested tissues were imaged for bioluminescence and fluorescence to determine lymphoma invasion and dissemination and PVX trafficking, respectively. Tissues were then frozen in OCT medium (Tissue-Tek, Sakura Finetek, USA) and stored at −80 °C for immunofluorescence and histology analysis. Tissue sections (10 μm thick) prepared on a Leica cryostat were fixed in ice-cold 95% (v/v) ethanol for 20 minutes, permeabilized using 0.2% (v/v) Triton-X in PBS for 2 min and blocked with 10% (v/v) goat serum for 1 hour. Sections were then stained with FITC-anti-CD45 antibody (Biolegend, San Diego, CA). Slides were mounted using Fluorshield with DAPI mounting media (Sigma) resulting in nuclear staining and sealed using nail polish and were stored at −20 °C. Stained sections were imaged on an Olympus Fluoview FV1000 confocal microscope.

PVX cell binding

PVX-Cy5 and PVX-Cys-Cy5 (5 μg) were added to 200 000 cells in each well and incubated for 1 hour on ice, in dark. Cells were washed twice with PBS with 3% (v/v) FBS and analyzed by flow cytometry on Attune NxT flow cytometer. Data was analyzed using the FlowJo software version 10.6.1.

Cell viability assay

Cells were plated at a concentration of 200 000 cells per mL using a clear-bottom 96-well cell culture plate and treated with 56 nM, 167 nM and 500 nM doses of vcMMAE and PVX–vcMMAE for 72 hours at 37 °C in a humidified atmosphere containing 5% CO_2. Cell viability and proliferation in cell lines were estimated using a resazurin-based assay (Prestoblue, Thermo Scientific) using instructions provided by the manufacturer. Cell viability in healthy B cells was measured using 7-AAD (Cayman Chemical Company, Ann Harbor, Michigan) cell-exclusion using flow cytometry analysis gated on the B cell fraction (CD19-PE, BD Biosciences, Franklin Lakes, New Jersey).

Drug delivery study and histology

NSG male mice (7 weeks) were inoculated with Raji-luc cells (1×10^6) intravenously. Mice were randomly split into 4 groups ($n = 5$): Vehicle (PBS), 0.125 mg kg^{-1} MMAE, 1 mg PVX (equivalent amount of PVX protein as used in the PVX–vcMMAE treatment group), and 0.4 mg kg^{-1} PVX–vcMMAE. For the first study, dosing started on day 3 and drug/drug delivery system were injected i.p. every 4th day for a total of 6 injections. For the second study, dosing started on day 11 and drug/drug delivery system were injected i.p. every 4th days for a total of 3 injections. For both studies, weekly bioluminescence imaging using the IVIS spectrum was used to monitor lymphoma progression. Survival of the mice was monitored and documented daily and mice were sacrificed when they either lost >15% of their body weight or showed signs of disease burden (hind leg paralysis). Tissues were harvested for histology using H&E staining to show tumor burden or lack thereof.

Statistical analysis

Statistical analysis was performed using the GraphPad Prism v8.2 software. For cell binding studies, statistical significance was determined using Ordinary one-way ANOVA and Tukey's multiple comparisons test (**** for $p < 0.0001$; *** for $p = 0.0001$; ** for $p < 0.01$ and * for $p < 0.05$). Survival data was plotted as Kaplan–Meier plot and analyzed with log-rank (Mantel–Cox) test.

Results and discussion

PVX was propagated in *Nicotiana benthamiana* plants and purified using a previously established protocol with yields of ~20 mg virus from 100 g of infected leaves.[27] PVX is a flexible filamentous nucleoprotein measuring 515 × 13 nm that is composed of 1270 identical copies of 25 kDa coat protein (CP) subunits. Each PVX coat protein has three solvent exposed lysine residues and one solvent exposed cysteine residue, which enables the conjugation of drugs, fluorescent dyes, peptides and imaging contrast agents *via* NHS or maleimide chemistries.[28–32] To investigate PVX-B lymphoma cell interactions *in vivo* and *in vitro*, fluorescently labeled PVX particles were prepared. PVX-Cy5 particles were synthesized by reacting NHS-sulfo-Cy5 with PVX (Fig. 1A). Using a dye/CP ratio of 0.5, ~190 dyes were conjugated per PVX particle. Dye labeling was confirmed through SDS-PAGE gel electrophoresis with appearance of the 25 kDa fluorescent band (Fig. S1, ESI†). Post-purification stability of PVX-Cy5 particles was confirmed using size exclusion chromatography that showed a characteristic elution profile with stable 260 : 280 ratios for PVX and co-elution of the fluorescent dye with the 260/280 peaks (Fig. 1B). PVX-Cys-Cy5 particles were synthesized similarly using maleimide-sulfo-Cy5 dyes and resulted in ~175 dyes per PVX.

We next evaluated PVX biodistribution in a mouse xenograft model of human NHL. Luciferase expressing Raji cells (Raji-luc), a human Burkitt lymphoma cell line, were injected intravenously into NOD/SCID/IL2-Rγ (NSG) female or male mice to establish the disease. Tumor progression was monitored *via in vivo* bioluminescence imaging. At day 27

†Electronic supplementary information (ESI) available. See DOI: 10.1039/d0bm00683a

from tumor inoculation, fluorescent PVX-Cy5 particles were injected intraperitoneally (i.p.) (5 mg kg^{-1}) in lymphoma bearing ($Raji^+$) male and female mice ($n = 3$) as well as healthy ($Raji^-$) mice (Fig. 1C). Mice were euthanized after 24 h and major organs were harvested for *ex vivo* bioluminescence and fluorescence imaging. The bioluminescence imaging of harvested tissues indicated lymphoma invasion primarily in the kidneys and lungs in male mice (Fig. 1D and Fig. S2, ESI†) and in the ovaries in female mice (Fig. 1E and Fig. S2, ESI†). Malignant lymphocytes migrate and recirculate similar to healthy B cells leading to dissemination in secondary sites including major organs such as lungs, kidneys, ovaries, spleens, bone marrow and lymph nodes.[33,34] The ovaries in lymphoma bearing female mice ($Raji^+$) were also significantly enlarged as compared to healthy mice ($Raji^-$) (Fig. 1E). PVX biodistribution observed through *ex vivo* fluorescence imaging of harvested tissues showed unexpected and interesting results: while PVX sequestration in the liver was observed as anticipated in all mice (Fig. S2, ESI†), in stark contrast to $Raji^-$ mice, the presence of PVX was observed in kidneys and ovaries of male and female $Raji^+$ mice, respectively, where the fluorescent signals co-localized with the bioluminescence from Raji-luc cells. Thus, in male $Raji^-$ mice, the liver and kidneys accounted for ~82% and ~7.4% of total PVX-Cy5 fluorescence signal, in $Raji^+$ mice a significant increase in proportion of signal (~20%) was detected from the kidneys. While lungs also showed an increased fluorescence in $Raji^+$ mice over $Raji^-$ mice, the difference was not statistically significant. Similarly, in female mice the percentage of PVX signal in ovaries rose sharply from ~1% in $Raji^-$ mice to ~8.5% in $Raji^+$ mice (Fig. S2, ESI†).

To further validate this observation, tissue sections stained with anti-human CD45 antibody were imaged using confocal microscopy. Both kidney and ovary sections showed some degree of co-localization of the PVX-Cy5 signals with that of human $CD45^+$ Raji cells (Mander's M2 values 0.54 and 0.56, respectively) (Fig. 1F and G). Moreover, no PVX fluorescence was observed in the kidney and ovary sections under confocal microscopy from $Raji^-$ mice (Fig. S3, ESI†), mirroring the *ex vivo* imaging data. Together, these results highlight the trafficking of PVX to tissues harboring disseminated B lymphoma cells in the NSG mouse model of human NHL.

Next, we validated PVX-B lymphoma cell interactions *in vitro*. Binding of fluorescent PVX particles (PVX-Cy5) to Raji cells was compared with a panel of cell lines including Daudi, panel of cell lines including Daudi (another human B lymphoma cell line), human myeloid leukemia cell lines HL60 and OCI-AML3, non-hematologic human cancer cell lines HCT-116 (colon cancer) and OVCAR-3 (ovarian cancer), and normal human B cells isolated from healthy donors (Fig. 2A). PVX particles were incubated with cells at 4 °C to assess cell binding while preventing cellular uptake. Post incubation, unbound particles were washed off and flow cytometry was used to detect Cy5 signal and determine the percentage of Cy5 positive cells. Under identical experimental conditions, PVX showed significantly stronger binding with the B cell lymphoma cell lines Raji and Daudi as compared to the other cell types tested. Specifically, PVX displayed a ~6 fold higher binding to Raji cells than HL60 cells, OCI-AML3 cells, and non-malignant B cells ($CD19^+$ normal B cells), ~4 fold higher binding than HCT-116 cells and ~30 fold higher binding than OVCAR-3 cells (Fig. 2A). These results suggest that PVX has a binding affinity towards malignant B cells and therefore support the observations made in biodistribution studies, where PVX accumulated

in lymphoma bearing tissues. At the same time, the significant difference in binding to malignant B cells *vs*. normal B cells could be advantageous when using PVX as a drug delivery vehicle, as it is likely to reduce off target drug toxicity in healthy B cells.

We also compared PVX-cell binding using PVX-Cys-Cy5 particles prepared by reacting sulfo-Cy5-maleimide dye with the sulfhydryl group of cysteine residues on the PVX coat protein and observed similar trend with PVX demonstrating higher binding with lymphoma cells compared to Normal B cells and other malignant cells (Fig. S4, ESI†).

Next, we investigated the potential of utilizing PVX as a targeted drug delivery system for B cell lymphoma using MMAE as the therapeutic payload. MMAE is a highly potent antimitotic agent with nearly 100× more potency than anthracyclines such as doxorubicin.[35,36] MMAE exerts its cytotoxic effects by binding to tubulin, causing G2/M cell cycle arrest, subsequently leading to apoptosis.[36] Though MMAE is a promising chemotherapeutic, it leads to acute systemic toxicity, thus requiring it to be administered as a safer pro-drug. The pro-drug Val-Cit linked MMAE (vcMMAE) is one of the current drugs being tested as a chemotherapeutic payload on ADCs in B cell lymphoma treatment. The vcMMAE formulation is stable under physiologic conditions, but undergoes rapid proteolytic cleavage in the catabolic microenvironment of lysosomes in cancer cells to release the free drug MMAE.[35,37] Previous data demonstrating endosomal trafficking of PVX supports the choice of this combination of drug payload and nanocarrier.[29,32] vcMMAE was conjugated to PVX's cysteine side chain making use of the maleimide handle of the vcMMAE pro-drug (Fig. 2B). A 7500 molar excess of vcMMAE was reacted with PVX overnight at 4 °C (at final concentration of 1 mg mL^{-1}). Post-synthesis, excess unconjugated drugs were separated as supernatant following ultracentrifugation. Re-suspended PVX–vcMMAE pellet was then purified further by overnight dialysis. PVX stability post drug conjugation was confirmed using transmission electron microscopy (TEM); TEM imaging shows the characteristic protein-based filaments measuring 515 × 13 nm (Fig. 2C). DLS analysis of PVX and PVX–vcMMAE showed comparable sizes (122 nm and 142 nm, respectively), indicating absence of aggregation and solution stability (Fig. S5, ESI†). SDS-PAGE confirmed covalent loading with vcMMAE as evident by a higher molecular weight band, i.e. >25 kDa (which is the native PVX coat protein, CP) (Fig. 2D). Protein band analysis using the Fiji/ImageJ software indicated ~30% of PVX CP conjugated with vcMMAE; or in other words, each PVX particle was loaded with ~400 vcMMAE molecules. SDS-PAGE followed by protein band analysis has been used to reliably quantify coat protein modifications for PVX and other viral nanoparticles.[18–20,38] We attempted to further increase drug loading, however increasing the vcMMAE/PVX molar ratios during synthesis led to particle aggregations and instability.

Next, we verified the *in vitro* cytotoxicity of PVX–vcMMAE drug conjugate. Comparison of cellular binding profile of PVX-Lys-Cy5 and PVX-Cys-Cy5 particles indicated that bioconjugation *via* cysteine residues did not alter the binding affinity of PVX and thus, vcMMAE conjugation was unlikely to significantly change PVX affinity towards malignant B cells. When incubated with increasing equivalent concentrations of free pro-drug vcMMAE and PVX–vcMMAE, B lymphoma cells displayed increased cytotoxicity with PVX–vcMMAE as compared to the free drug (Fig. 2E). The dose proportional toxicity of

PVX–vcMMAE is further supported by the significantly lower IC_{50} values (50 nM and 23 nM for Raji and Daudi cells, respectively) over the IC_{50} values of vcMMAE (160 nM and 80 nM in Raji and Daudi cells, respectively). As discussed, the pro-drug vcMMAE needs to undergo proteolytic cleavage to release the active form MMAE. As the free pro-drug uptake is limited and inefficient, PVX delivery enables an increase in potency of vcMMAE. It is important to note, that soluble vcMMAE and PVX–vcMMAE both displayed no cytotoxicity towards the non-dividing normal donor B cells (Fig. 2E). Auristatin drugs only kill rapidly dividing cells by inducing mitotic arrest.[36]

Finally, we evaluated the therapeutic potential of PVX–vcMMAE *in vivo* using a Raji B cell lymphoma model in NSG mice. Male NSG mice were injected intravenously with luciferase expressing Raji cells and monitored for lymphoma engraftment and progression using bioluminescence imaging. Tumor engrafted mice were randomly assigned to the treatment groups ($n = 5$). Starting on day 3 post-tumor challenge, mice were treated 6 times at four-day intervals with PVX (1 mg), PVX–vcMMAE (0.4 mg kg^{-1}; based on 1 mg PVX), MMAE (0.125 mg kg^{-1}), or PBS (Fig. 3A). The MMAE dose was selected based on the fact that the known maximum tolerated dose (MTD) of free MMAE is 0.25–0.5 mg kg^{-1} after a single administration.[35,39] A dose of 0.125 mg kg^{-1} was chosen to allow for multiple treatments. Mice injected intravenously with Raji cells develop hind leg paralysis (due to the infiltration of neoplastic cells into the spinal canal) and/or lose weight prior to death.[40] Therefore, hind leg paralysis and/or >15% loss in body weight were considered experimental endpoints at which mice were euthanized.

As observed in the biodistribution studies, bioluminescence imaging indicated early signs of lymphoma in kidneys and subsequent dissemination to other regions, such as spleen, lungs and the CNS (Fig. 3B). As evident by bioluminescence intensities, lymphoma progressed rapidly between days 12–24 in the PBS and PVX treatment groups and was widespread by day 38 (Fig. 3C). The median survival for PBS treated mice was 45 days, which is consistent with previous reports.[33,34] As expected, PVX nanocarrier treatment alone had no effect on disease progression (median survival of 54 days *vs.* 45 for PBS treatment; $p = 0.0527$) (Fig. 3D). As evident from bioluminescence imaging and survival data, soluble MMAE treatment partially limited lymphoma progression and improved median survival to 61 days ($p = 0.009$ *vs.* PBS treatment) (Fig. 3C and D); this limited effect can be explained by the insufficient dosing with soluble MMAE, limited by the inherent toxicities of this drug. In stark contrast, the PVX–vcMMAE group significantly impaired the progression of lymphoma as evidenced by bioluminescent imaging as well as an increase in overall survival; the median survival was 74 days ($p = 0.0002$ *vs.* PBS; $p = 0.0134$ *vs.* MMAE; $p = 0.0134$ *vs.* PVX). The efficacy of treatment was dependent on the number of doses and treatment schedules. In a separate study involving fewer doses and delayed treatment (three doses starting at day 11 post-tumor challenge), the median survival of PVX–vcMMAE treatment group was 56 days *vs.* 42 days for PBS treated mice ($p = 0.037$) (Fig. S6, ESI†). In comparison, MMAE and PVX treatment showed no improvement in overall survival to PBS treatment (median survival of 39 days for MMAE and 46 days for PVX with $p = 0.3513$ and $p = 0.2691$ *vs.* PBS treatment, respectively). Thus, PVX–vcMMAE clearly outperformed MMAE in its soluble form.

Histological analysis performed on mouse kidney sections further corroborated these observations (Fig. 3E). Kidneys were harvested from PBS, PVX and MMAE treated mice that were all sacrificed when they became moribund, whereas kidneys from the PVX–vcMMAE treated mice were isolated at the end of study period. Histological sections from the PBS and PVX treatment groups showed the presence of large areas infiltrated by lymphoma cells (dark stained regions) as compared to the MMAE treated group that showed reduced lymphoma cell infiltration. On the other hand, kidney sections from the PVX–vcMMAE treatment group show significantly reduced lymphomas at the end of study period. Therefore the data indicates that PVX may be a suitable carrier for drug delivery targeting NHL.

Together, we have demonstrated the potential of filamentous PVX carriers to be engineered for drug delivery and the treatment of NHL in a mouse model. This plant virus-based drug delivery platform offers several advantages over contemporary nanotechnology approaches targeting NHL. PVX can be produced in high yields using simple molecular farming methods and offers the safety of non-infectious and non-replicating viral technology for mammalian use.[17,27] As compared to synthetic nanoparticles, PVX nanofilaments offer unique flexible nanoparticle morphology, which is difficult to synthesize using purely chemical approaches. Further, compared to ADCs, PVX can carry a higher payload and home to target sites with shorter circulation times, possibly preventing premature release and off-target toxicities. And finally, the B cell homing properties of the PVX nanostructures may bypass the need for additional targeting strategies.

Further research is required to probe the PVX–NHL interactions and to delineate whether there is specific, molecular targeting or whether the phenomenon is a result of the shape and size of the PVX nanocarrier. Mammalian viruses such as Epstein–Barr virus have been known to bind B cells through surface glycoprotein.[41,42] It is not known how PVX interacts with B cells; however some data suggests PVX may be glycosylated[43,44] and therefore glycosylation may be driving the B cell binding. Indeed, other examples have shown that plant viruses can have specificity toward mammalian cells and proteins. For example, previous data show that Cowpea mosaic virus interacts with mammalian cells through surface vimentin,[45,46] a trait that it shares with several mammalian viruses.[47–49] Therefore, the B cell tropism in PVX could be derived from a protein–protein interaction.

In conclusion, we demonstrate PVX homing to malignant B cells, which makes PVX a promising drug delivery platform nanotechnology for B cell lymphomas. Further mechanistic insights into these interactions will enable the development of other targeted therapeutics and nanotechnologies.

Supplementary Material

Refer to Web version on PubMed Central for supplementary material.

Acknowledgements

This work was funded in part by a Research Scholar Grant from the American Cancer Society (128319-RSG-15-144-01-CDD to N. F. S.). This research was also supported in part by the Hematopoietic Biorepository and

Cellular Therapy and Athymic Animal Shared Resources of the Case Comprehensive Cancer Center (P30CA043703). We would like to acknowledge Paul Laurent Chariou (UC San Diego) for TEM imaging.

References

1. Howlader N, Mariotto AB, Besson C, Suneja G, Robien K, Younes N and Engels EA, Cancer, 2017, 123, 3326–3334. [PubMed: 28464214]
2. Siegel RL, Miller KD and Jemal A, CA Cancer J. Clin, 2018, 68, 7–30. [PubMed: 29313949]
3. Cheson BD, Blood, 2016, 128, 325–330. [PubMed: 27222479]
4. Hodgson DC, Clin. Adv. Hematol. Oncol, 2015, 13, 103–112. [PubMed: 25774480]
5. Dalton WS, Grogan TM, Meltzer PS, Scheper RJ, Durie BG, Taylor CW, Miller TP and Salmon SE, J. Clin. Oncol, 1989, 7, 415–424. [PubMed: 2564428]
6. Farooq U, Maurer MJ, Thompson CA, Thanarajasingam G, Inwards DJ, Micallef I, Macon W, Syrbu S, Lin T, Lin Y, Ansell SM, Nowakowski GS, Habermann TM, Cerhan JR and Link BK, Br. J. Haematol, 2017, 179, 50–60. [PubMed: 28653407]
7. Beck A, Goetsch L, Dumontet C and Corvaia N, Nat. Rev. Drug Discovery, 2017, 16, 315–337. [PubMed: 28303026]
8. Jagadeesh D and Smith MR, Curr. Treat. Options Oncol, 2016, 17, 55. [PubMed: 27544507]
9. McCombs JR and Owen SC, AAPS J., 2015, 17, 339–351. [PubMed: 25604608]
10. Alley SC, Okeley NM and Senter PD, Curr. Opin. Chem. Biol, 2010, 14, 529–537. [PubMed: 20643572]
11. Farokhzad OC and Langer R, ACS Nano, 2009, 3, 16–20. [PubMed: 19206243]
12. Li HJ, Du JZ, Du XJ, Xu CF, Sun CY, Wang HX, Cao ZT, Yang XZ, Zhu YH, Nie S and Wang J, Proc. Natl. Acad. Sci. U. S. A, 2016, 113, 4164–4169. [PubMed: 27035960]
13. Zhou S, Wu D, Yin X, Jin X, Zhang X, Zheng S, Wang C and Liu Y, J. Exp. Clin. Cancer Res, 2017, 36, 24. [PubMed: 28166836]
14. Qiu L, Dong C and Kan X, Drug Des., Dev. Ther, 2018, 12, 863–872.
15. Zhu B, Yu L and Yue Q, Biomed. Pharmacother, 2017, 91, 287–294. [PubMed: 28463792]
16. Xu P, Zuo H, Chen B, Wang R, Ahmed A, Hu Y and Ouyang J, Sci. Rep, 2017, 7, 42632. [PubMed: 28198453]
17. Wen AM and Steinmetz NF, Chem. Soc. Rev, 2016, 45, 4074–4126. [PubMed: 27152673]
18. Cai H, Shukla S, Wang C, Masarapu H and Steinmetz NF, J. Am. Chem. Soc, 2019, 141, 6509–6518. [PubMed: 30995022]
19. Hu H, Masarapu H, Gu Y, Zhang Y, Yu X and Steinmetz NF, ACS Appl. Mater. Interfaces, 2019, 11, 18213–18223. [PubMed: 31074602]
20. Le DHT, Commandeur U and Steinmetz NF, ACS Nano, 2019, 13, 2501–2510. [PubMed: 30668110]
21. Kim H, Choi H, Bae Y and Kang S, Biotechnol. Bioeng, 2019, 116, 2843–2851. [PubMed: 31329283]
22. Thong QX, Biabanikhankahdani R, Ho KL, Alitheen NB and Tan WS, Sci. Rep, 2019, 9, 3945. [PubMed: 30850643]
23. Shukla S, Ablack AL, Wen AM, Lee KL, Lewis JD and Steinmetz NF, Mol. Pharm, 2013, 10, 33–42. [PubMed: 22731633]
24. Shukla S, Wen AM, Ayat NR, Commandeur U, Gopalkrishnan R, Broome AM, Lozada KW, Keri RA and Steinmetz NF, Nanomedicine, 2014, 9, 221–235. [PubMed: 23834501]
25. Shukla S, Myers JT, Woods SE, Gong X, Czapar AE, Commandeur U, Huang AY, Levine AD and Steinmetz NF, Biomaterials, 2017, 121, 15–27. [PubMed: 28063980]
26. Campeau E, Ruhl VE, Rodier F, Smith CL, Rahmberg BL, Fuss JO, Campisi J, Yaswen P, Cooper PK and Kaufman PD, PLoS One, 2009, 4, e6529. [PubMed: 19657394]
27. Shukla S, Dickmeis C, Fischer R, Commandeur U and Steinmetz NF, Methods Mol. Biol, 2018, 1776, 61–84. [PubMed: 29869235]

28. Le DHT, Hu H, Commandeur U and Steinmetz NF, J. Struct. Biol, 2017, 200, 360–368. [PubMed: 28647539]
29. Steinmetz NF, Mertens ME, Taurog RE, Johnson JE, Commandeur U, Fischer R and Manchester M, Nano Lett., 2010, 10, 305–312. [PubMed: 20017489]
30. Lee KL, Shukla S, Wu M, Ayat NR, El Sanadi CE, Wen AM, Edelbrock JF, Pokorski JK, Commandeur U, Dubyak GR and Steinmetz NF, Acta Biomater., 2015, 19, 166–179. [PubMed: 25769228]
31. Lee KL, Uhde-Holzem K, Fischer R, Commandeur U and Steinmetz NF, Methods Mol. Biol, 2014, 1108, 3–21. [PubMed: 24243237]
32. Shukla S, DiFranco NA, Wen AM, Commandeur U and Steinmetz NF, Cell. Mol. Bioeng, 2015, 8, 433–444. [PubMed: 26316894]
33. Chao MP, Tang C, Pachynski RK, Chin R, Majeti R and Weissman IL, Blood, 2011, 118, 4890–4901. [PubMed: 21828138]
34. Donnou S, Galand C, Touitou V, Sautes-Fridman C, Fabry Z and Fisson S, Adv. Hematol, 2012, 2012, 701704. [PubMed: 22400032]
35. Qi R, Wang Y, Bruno PM, Xiao H, Yu Y, Li T, Lauffer S, Wei W, Chen Q, Kang X, Song H, Yang X, Huang X, Detappe A, Matulonis U, Pepin D, Hemann MT, Birrer MJ and Ghoroghchian PP, Nat. Commun, 2017, 8, 2166. [PubMed: 29255160]
36. Waight AB, Bargsten K, Doronina S, Steinmetz MO, Sussman D and Prota AE, PLoS One, 2016, 11, e0160890.
37. Yu SF, Zheng B, Go M, Lau J, Spencer S, Raab H, Soriano R, Jhunjhunwala S, Cohen R, Caruso M, Polakis P, Flygare J and Polson AG, Clin. Cancer Res, 2015, 21, 3298–3306. [PubMed: 25840969]
38. Pitek AS, Jameson SA, Veliz FA, Shukla S and Steinmetz NF, Biomaterials, 2016, 89, 89–97. [PubMed: 26950168]
39. Francisco JA, Cerveny CG, Meyer DL, Mixan BJ, Klussman K, Chace DF, Rejniak SX, Gordon KA, DeBlanc R, Toki BE, Law CL, Doronina SO, Siegall CB, Senter PD and Wahl AF, Blood, 2003, 102, 1458–1465. [PubMed: 12714494]
40. Lapalombella R, Zhao X, Triantafillou G, Yu B, Jin Y, Lozanski G, Cheney C, Heerema N, Jarjoura D, Lehman A, Lee LJ, Marcucci G, Lee RJ, Caligiuri MA, Muthusamy N and Byrd JC, Clin. Cancer Res, 2008, 14, 569–578. [PubMed: 18223233]
41. Nemerow GR, Houghten RA, Moore MD and Cooper NR, Cell, 1989, 56, 369–377. [PubMed: 2464439]
42. Tanner J, Weis J, Fearon D, Whang Y and Kieff E, Cell, 1987, 50, 203–213. [PubMed: 3036369]
43. Baratova LA, Fedorova NV, Dobrov EN, Lukashina EV, Kharlanov AN, Nasonov VV, Serebryakova MV, Kozlovsky SV, Zayakina OV and Rodionova NP, Eur. J. Biochem, 2004, 271, 3136–3145. [PubMed: 15265033]
44. Tozzini AC, Ek B, Palva ET and Hopp HE, Virology, 1994, 202, 651–658. [PubMed: 8030230]
45. Koudelka KJ, Destito G, Plummer EM, Trauger SA, Siuzdak G and Manchester M, PLoS Pathog., 2009, 5, e1000417.
46. Koudelka KJ, Rae CS, Gonzalez MJ and Manchester M, J. Virol, 2007, 81, 1632–1640. [PubMed: 17121801]
47. Das S, Ravi V and Desai A, Virus Res., 2011, 160, 404–408. [PubMed: 21798293]
48. Du N, Cong H, Tian H, Zhang H, Zhang W, Song L and Tien P, J. Virol, 2014, 88, 5816–5833. [PubMed: 24623428]
49. Yu YT, Chien SC, Chen IY, Lai CT, Tsay YG, Chang SC and Chang MF, J. Biomed. Sci, 2016, 23, 14. [PubMed: 26801988]

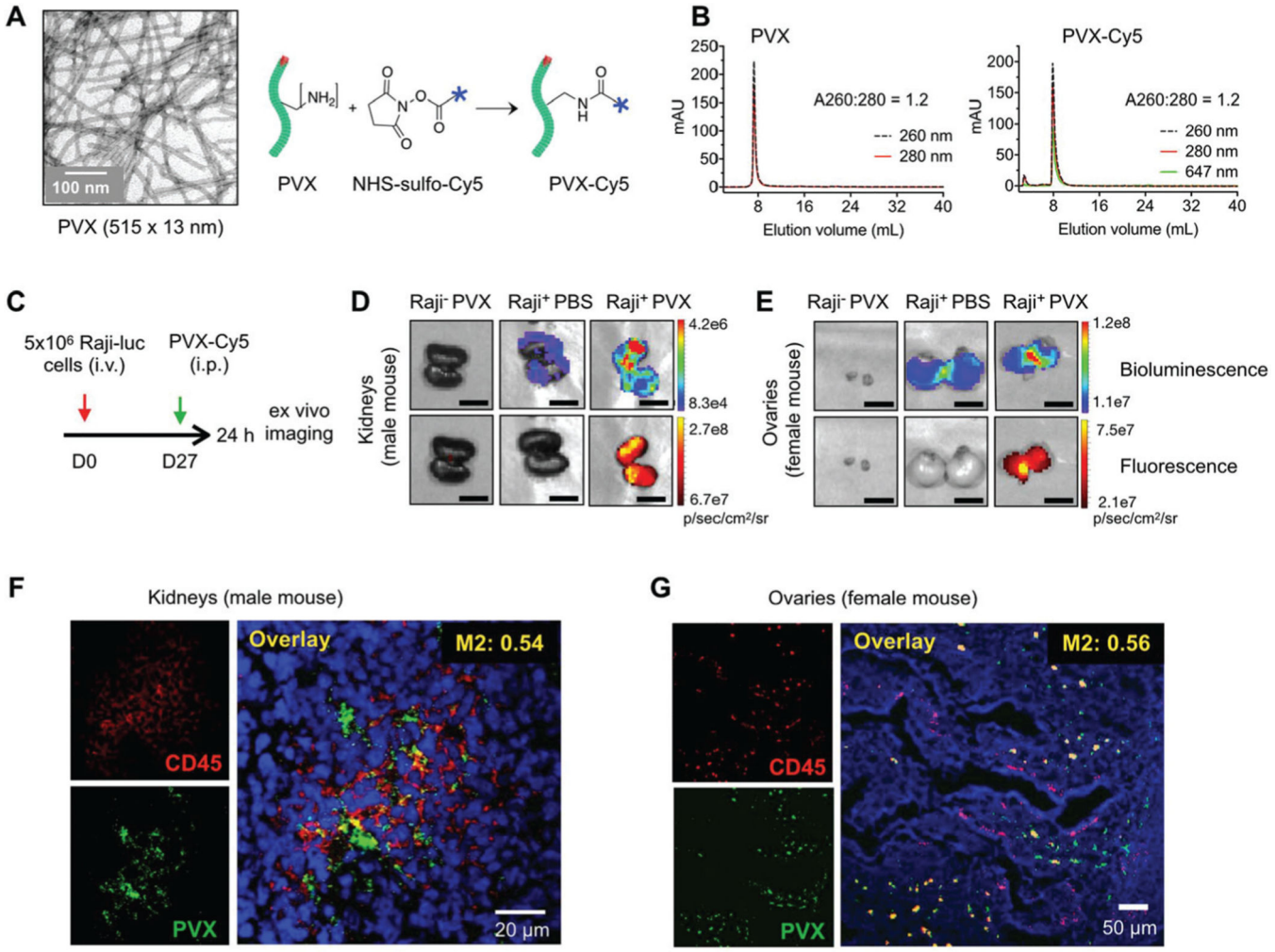

Fig. 1.

PVX biodistribution and tumor homing in a NHL mouse model: (A) PVX nanofilaments (515 × 13 nm) are composed of 1270 identical copies of a 25 kDa coat protein (green) wrapped around a single-stranded RNA (red). PVX was conjugated with Cy5 dyes *via* the Lys residues on the CP using NHS-chemistry. (B) Dye conjugation and particle integrity was confirmed using size exclusion chromatography analysis of elution profiles and A_{260} : A_{280} ratios of PVX and PVX-Cy5. (C) Biodistribution and lymphoma homing of PVX was studied by inoculating male and female NSG mice with 5×10^6 Raji-luc B lymphoma cells *via* intravenous injections. On day 27 post-tumor challenges, 100 µg PVX-Cy5 particles were administered *via* intraperitoneal injection followed by *ex vivo* bioluminescence and fluorescence imaging. (D) PVX trafficking to kidneys in male and ovaries in female mice (E) was compared in Raji lymphoma bearing $Raji^+$ and healthy $Raji^-$ mice through colocalization of bioluminescence signal (Raji-luc cells) and fluorescence (PVX-Cy5). (F and G) PVX trafficking to Raji B lymphoma cells in kidney and ovaries was also confirmed by confocal microscopy performed on tissue sections stained for $CD45^+$ Raji cells.

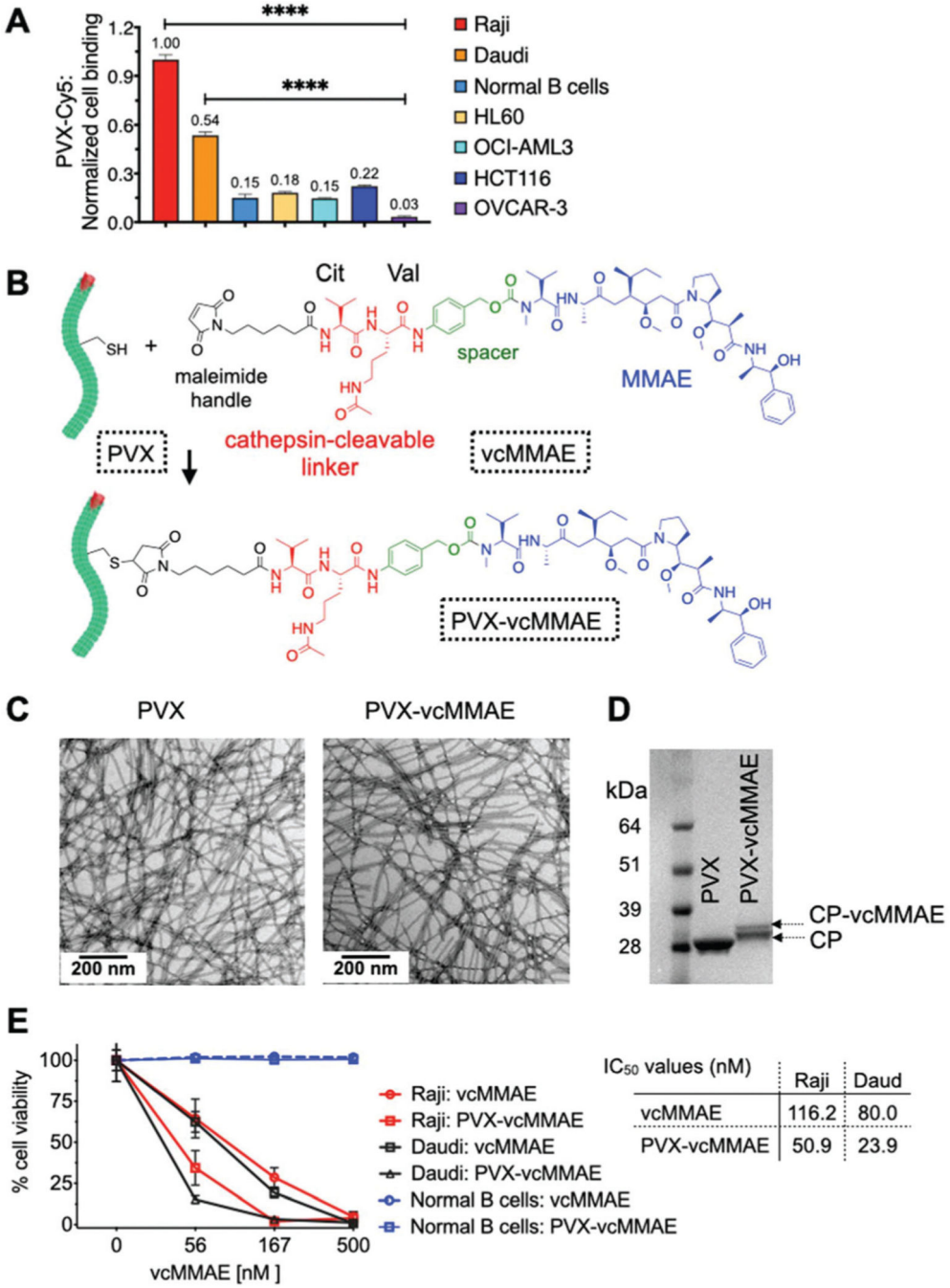

Fig. 2.

PVX-B lymphoma cell interactions and PVX–vcMMAE cytotoxicity: (A) PVX cell interactions were evaluated through *in vitro* cell binding of PVX-Cy5 particles using a panel of cells with flow cytometry; statistical analysis was performed using ordinary one-way ANOVA (Tukey's multiple comparison tests; **** $p < 0.0001$). (B) vcMMAE was conjugated to PVX *via* the cysteine residues using the maleimide chemistry leading to formation of PVX–vcMMAE. (C) TEM was used to verify the structural integrity of PVX post modification. (D) vcMMAE conjugation was assessed by SDS-PAGE. (E) Cell viability

assays were used to determine cytotoxicity of PVX–vcMMAE and vcMMAE pro-drug in Raji and Daudi lymphoma cells, and normal B cells derived from healthy human donor. IC_{50} values were calculated using GraphPad Prism software.

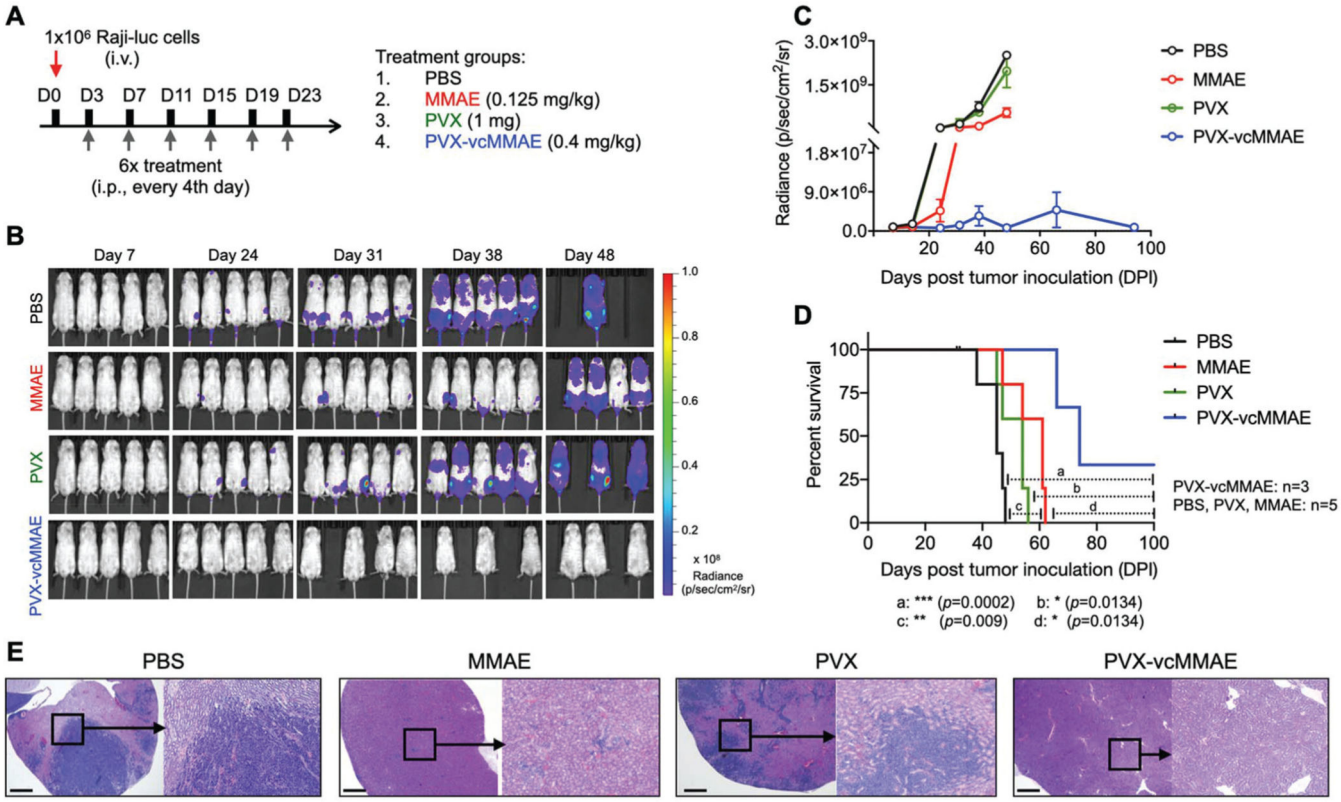

Fig. 3.

Therapeutic efficacy of PVX–vcMMAE: (A) Raji B cell lymphoma model in NSG mice was used to determine the therapeutic efficacy of PVX–vcMMAE. Mice engrafted with 1×10^6 Raji-Luc B lymphoma cells were treated six times at four-day intervals with PBS, PVX, MMAE and PVX–vcMMAE and tumor progression was monitored using bioluminescence imaging (B and C). Treatment efficacy was measured *via* overall survival (D) and histological analysis of kidney sections were used to highlight the efficacy of various treatments (E). The scale bars in (E) are 0.2 mm. Survival curves were analyzed using the log-rank Mantel–Cox test using GraphPad Prism8 software. 2 mice were lost during the study; these mice had no signs of lymphoma. Whether these mice experienced treatment-related side effects is not clear; no weight loss was observed.